

Hamiltonian Truncation Study of the ϕ^4 Theory in Two Dimensions

II. The \mathbb{Z}_2 -Broken Phase and the Chang Duality

Slava Rychkov^{a,b,c}, Lorenzo G. Vitale^d

^a CERN, Theory Department, Geneva, Switzerland

^b Laboratoire de Physique Théorique de l'École normale supérieure (LPTENS), Paris, France

^c Sorbonne Universités, UPMC Univ Paris 06, Faculté de Physique, Paris, France

^d Institut de Théorie des Phénomènes Physiques, EPFL, CH-1015 Lausanne, Switzerland

Abstract

The Fock-space Hamiltonian truncation method is developed further, paying particular attention to the treatment of the scalar field zero mode. This is applied to the two-dimensional ϕ^4 theory in the phase where the \mathbb{Z}_2 -symmetry is spontaneously broken, complementing our earlier study of the \mathbb{Z}_2 -invariant phase and of the critical point. We also check numerically the weak/strong duality of this theory discussed long ago by Chang.

December 2015

Contents

1	Introduction	3
2	The Chang duality	4
2.1	Formulation and consequences	4
2.2	Review of the derivation	5
2.3	Numerical check of the duality	6
2.3.1	Direct theory	6
2.3.2	Dual theory	8
2.3.3	Comparison	9
3	The \mathbb{Z}_2-broken phase	10
3.1	Modified zero mode treatment	10
3.2	Varying the normal-ordering mass	12
3.3	Results	13
3.3.1	Perturbative sector	13
3.3.2	Non-perturbative sector	14
3.3.3	Comparison to Ref. [3]	17
4	Conclusions	19
A	Renormalization in the \mathbb{Z}_2-broken phase	20
B	Perturbation theory checks	21
C	Ground state splitting	23

1 Introduction

The two-dimensional ϕ^4 theory is perhaps the simplest quantum field theory (QFT) which is not exactly solvable. It is thus an ideal laboratory for studying approximate solution techniques. In our recent paper [1], we studied this theory using the method of *Hamiltonian truncation*—a QFT analogue of the Rayleigh-Ritz method in quantum mechanics. In that work, we considered the case of positive bare mass $m^2 > 0$ and of quartic coupling $g = \bar{g}m^2$ with $\bar{g} = O(1)$. The physical particle mass is given by

$$m_{\text{ph}} = f(\bar{g})m, \tag{1.1}$$

and the function $f(\bar{g})$ was determined numerically. We observed that the physical mass vanishes for $\bar{g} = \bar{g}_c \approx 3$, signaling the presence of a second order phase transition.

In [1], our focus was mainly on the region below and around the critical coupling \bar{g}_c . In this second work of the series we will instead be interested in the complementary region $\bar{g} > \bar{g}_c$. In this range of couplings the theory is massive, but the \mathbb{Z}_2 symmetry, $\phi \rightarrow -\phi$, is spontaneously broken. In infinite volume, there are therefore two degenerate vacua, and two towers of massive excitations around them.

We will be able to determine the low energy spectrum as a function of \bar{g} . In finite volume the exact degeneracy is lifted, and the energy eigenstates come in pairs split by a small amount, exponentially small if the volume is large. In this paper, as in [1], we will regulate the theory by putting it in finite volume.

In the \mathbb{Z}_2 -broken phase, there is also a topologically nontrivial sector of “kink” states corresponding, in the semiclassical limit, to field configurations interpolating between the two vacua. In this work we will probe the kink mass by studying the mass splittings in the topologically trivial sector. In the future it would be interesting to study the kink sector directly.

One interesting feature of the theory under study is that it enjoys a weak/strong coupling duality first discussed by Chang [2]. The dual description exists for all $\bar{g} \geq \bar{g}_* \approx 2.26$. As we review below, the duality relates a description in which the theory is quantized around the \mathbb{Z}_2 -invariant vacuum state to an equivalent description in which it is quantized around a \mathbb{Z}_2 -breaking vacuum. For \bar{g} not much above \bar{g}_* both descriptions are strongly coupled¹ and they can be equivalently employed as a starting point for the numerical computations. In section 2 we present a comparison between the numerical spectra obtained using the two descriptions, serving both as a non-trivial test of the method and as a check of the Chang duality.

On the other hand, for $\bar{g} \gg \bar{g}_*$ the dual description becomes weakly coupled, and provides the better starting point. In section 3, we will explain a modification of the method which can be used, among other things, to study this regime (a weakly coupled ϕ^4 theory with negative m^2) efficiently. It is based on a different treatment of the zero mode of the field. We will compare the numerical results with the predictions from perturbation theory and from semiclassical analyses.

We conclude in section 4. Several technical details are relegated to the appendices.

Recently, the \mathbb{Z}_2 -broken phase of the two-dimensional ϕ^4 model was studied in Ref. [3] using

¹This explains why \bar{g}_* need not be equal, and in fact is not equal to the critical coupling \bar{g}_c mentioned above.

a version of the Truncated Conformal Space Approach [4, 5]. Differences and similarities between our works will be mentioned throughout the paper.

2 The Chang duality

2.1 Formulation and consequences

According to Chang [2], the two-dimensional ϕ^4 theory described by the (Euclidean) Lagrangian

$$\mathcal{L} = \frac{1}{2}(\partial\phi)^2 + \frac{1}{2}m^2\phi^2 + g N_m(\phi^4) \quad (2.1)$$

with $m^2 > 0$, $g > 0$, admits a dual description in terms of a Lagrangian with a different, and negative, value of the squared mass:

$$\mathcal{L}' = \frac{1}{2}(\partial\phi)^2 - \frac{1}{4}M^2\phi^2 + g N_M(\phi^4). \quad (2.2)$$

The actual value of the dual mass will be given below.

Note that the duality is between quantum theories in the continuum limit, and to specify this limit one has to subtract the logarithmic divergence of the mass parameters. The divergence is removed by normal-ordering the quartic interaction with respect to the mass indicated in the subscript of the normal ordering sign N . The potential in \mathcal{L}' has two minima at $\phi = c = \pm M/\sqrt{8g}$. After the shift $\phi \rightarrow \phi + c$ the dual Lagrangian becomes²

$$\mathcal{L}' \rightarrow \frac{1}{2}(\partial\phi)^2 + \frac{1}{2}M^2\phi^2 + \sqrt{2g}M N_M(\phi^3) + g N_M(\phi^4). \quad (2.3)$$

In this way of writing, interactions of both \mathcal{L} and \mathcal{L}' are normal ordered with respect to the mass appearing in the quadratic part of the Lagrangian. In perturbation theory such normal ordering means that we are simply forbidding diagrams with the lines starting and ending in the same vertex.

To find the dual mass M^2 , one is instructed to solve the equation:

$$F(X) = f(x), \quad (2.4)$$

where $x = g/m^2$, $X = g/M^2$ are the dimensionless quartic couplings of the two descriptions (x is given and X is an unknown) and

$$f(x) \equiv \log x - \pi/(3x), \quad F(X) \equiv \log X + \pi/(6X). \quad (2.5)$$

This equation is illustrated in Fig. 1. There is no solution for

$$x < x_* = \frac{\pi}{3W(2/e)} \approx 2.26149, \quad (2.6)$$

where $W(z)$ is the Lambert W function. For $x \geq x_*$ there are two solution branches. We are particularly interested in the lower branch $X_1(x)$, which for large x approaches zero:

$$X_1(x) \approx \pi/(6 \log x), \quad x \rightarrow \infty. \quad (2.7)$$

²Notice that normal ordering is a linear operation, and thus commutes with the field shift.

The dual description corresponding to this branch becomes weakly coupled in the limit in which the original description becomes stronger and stronger coupled. We thus have a weak/strong coupling duality.

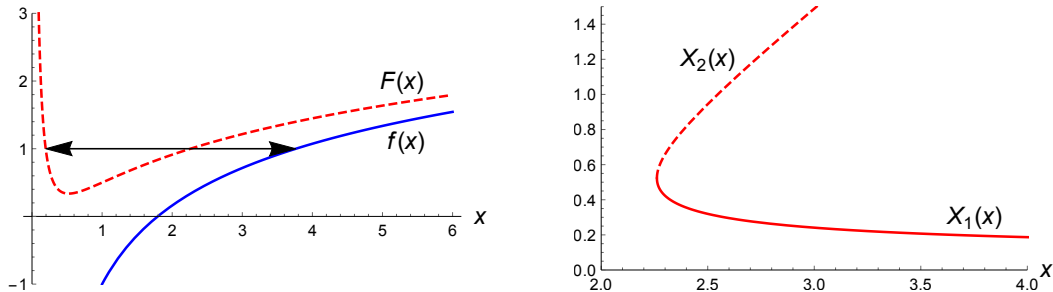


Figure 1: Left panel: equation $F(X) = f(x)$ has two solutions for $x > x_*$. Right panel: the two solution branches $X_{1,2}(x)$. We are mostly interested in the lower branch $X_1(x)$ which becomes weakly coupled as $x \rightarrow \infty$.

Chang [2] used this duality to show that the ϕ^4 theory undergoes a phase transition. Indeed, for small x we can use perturbation theory to argue that the theory is in the symmetric phase, with the \mathbb{Z}_2 symmetry $\phi \rightarrow -\phi$ unbroken. On the other hand, for large x we use the dual description. Since in that description the potential is a double well, and moreover the dual coupling is weak for $x \gg 1$, we conclude that for large x the \mathbb{Z}_2 symmetry is spontaneously broken. By continuity, there must be a phase transition at an intermediate value of x .

This argument does not establish whether the transition is first or second order. However, as explained in [2], a first order transition is excluded by rigorous theorems due to Simon and Griffiths [6]. So the transition must be second order. This conclusion is supported by Monte Carlo simulations [7–10], as well as by computations using DLCQ [11], density matrix renormalization group [12], matrix product states [13], and the Hamiltonian truncation [14, 15, 1].

Nor does the above argument predict the value of x at which the phase transition must happen. In particular, the fact that the dual description exists at $x \geq x_*$ does not mean that the phase transition happens at $x = x_*$. Indeed, at $x = x_*$ both the direct and the dual descriptions are strongly coupled, and the fate of the \mathbb{Z}_2 symmetry is not *a priori* clear. In fact, calculations indicate a higher phase transition location at $x_c \approx 2.75 - 3$ [1, 9, 13, 10, 16].

2.2 Review of the derivation

Here’s a quick derivation of the Chang duality, following [2]. We will work in the Hamiltonian formalism, and consider the normal-ordered Hamiltonians corresponding to \mathcal{L} and \mathcal{L}' :

$$H = \int dx N_m \left(\frac{1}{2} \dot{\phi}^2 + \frac{1}{2} \phi'^2 + \frac{1}{2} m^2 \phi^2 + g \phi^4 \right), \quad (2.8)$$

$$H' = \int dx N_M \left(\frac{1}{2} \dot{\phi}^2 + \frac{1}{2} \phi'^2 - \frac{1}{4} M^2 \phi^2 + g \phi^4 + \Lambda \right). \quad (2.9)$$

Notice that we are now normal ordering the full Hamiltonian, including the quadratic part. This more careful procedure will allow us to establish the correspondence also for the ground state energy. In the dual description it will receive an extra constant contribution, denoted Λ in (2.9).

Recall Coleman [17] relations between normal orderings with respect to different masses:

$$\begin{aligned} N_m(\tfrac{1}{2}\dot{\phi}^2 + \tfrac{1}{2}\phi'^2) &= N_M(\tfrac{1}{2}\dot{\phi}^2 + \tfrac{1}{2}\phi'^2) + Y, \\ N_m(\phi^2) &= N_M(\phi^2) + Z, \\ N_m(\phi^4) &= N_M(\phi^4) + 6ZN_M(\phi^2) + 3Z^2, \end{aligned} \tag{2.10}$$

where $Y = Y(m, M)$ and $Z = Z(m, M)$ are the differences of the normal-ordering constants.³

$$\begin{aligned} Y(m, M) &= \int \frac{dk}{8\pi} \left\{ \frac{2k^2 + M^2}{\sqrt{k^2 + M^2}} - (M \rightarrow m) \right\} = \frac{1}{8\pi}(M^2 - m^2), \\ Z(m, M) &= \int \frac{dk}{4\pi} \left\{ \frac{1}{\sqrt{k^2 + M^2}} - (M \rightarrow m) \right\} = \frac{1}{4\pi} \log \frac{m^2}{M^2}. \end{aligned} \tag{2.11}$$

Using these relations, one can see that H maps on H' as long as

$$\tfrac{1}{2}m^2 + 6Zg = -\tfrac{1}{4}M^2, \tag{2.12}$$

written equivalently as (2.4). We also find a constant contribution to the ground state energy

$$\Lambda = Y + \tfrac{1}{2}m^2Z + 3gZ^2. \tag{2.13}$$

2.3 Numerical check of the duality

We will test the Chang duality by comparing the spectra of the direct and dual theories in a finite volume—a circle of length L . The spectra will be computed using the Hamiltonian truncation. We will first describe the setup for these computations, and then present the results.

2.3.1 Direct theory

By the direct theory we mean (2.8) put on a circle of length L . This is precisely the theory we were studying in [1], and we will be following the same method. Here we will give just a brief reminder. The finite volume Hamiltonian corresponding to the infinite-volume Hamiltonian (2.8) is given in [1], Eq. (2.19), and has the form:

$$H(L) = H_0 + g[V_4 + 6\zeta V_2] + [E_0 + 3\zeta^2 gL], \tag{2.14}$$

Here H_0 is the Hamiltonian of the free scalar field on the circle:

$$H_0(L, m) = \sum_k \omega(k) a_k^\dagger a_k, \quad k = (2\pi/L)n, \quad n \in \mathbb{Z}, \quad \omega(k) = \sqrt{m^2 + k^2}, \tag{2.15}$$

³The expression for Z can also be equivalently derived in the Lagrangian language as the difference of one-loop massive diagrams: $Z = \int \frac{d^2k}{(2\pi)^2} \left(\frac{1}{k^2 + M^2} - \frac{1}{k^2 + m^2} \right)$.

where a, a^\dagger are the ladder operators appearing in the field mode expansion:

$$\phi(x) = \sum_k \frac{1}{\sqrt{2L\omega(k)}} \left(a_k e^{ikx} + a_k^\dagger e^{-ikx} \right). \quad (2.16)$$

The V_4 term is the normal ordered quartic interaction:

$$V_4(L, m) = \frac{1}{L} \sum_{\sum k_i=0} \frac{1}{\prod \sqrt{2\omega(k_i)}} \left[(a_{k_1} a_{k_2} a_{k_3} a_{k_4} + 4a_{-k_1}^\dagger a_{k_2} a_{k_3} a_{k_4} + \text{h.c.}) + 6a_{-k_1}^\dagger a_{-k_2}^\dagger a_{k_3} a_{k_4} \right]. \quad (2.17)$$

The other terms in (2.14) are all exponentially suppressed for $Lm \gg 1$. In particular,

$$E_0(L, m) = -\frac{1}{\pi L} \int_0^\infty dx \frac{x^2}{\sqrt{m^2 L^2 + x^2}} \frac{1}{e^{\sqrt{m^2 L^2 + x^2}} - 1}. \quad (2.18)$$

is the Casimir energy of the free scalar field in finite volume. Corrections involving

$$\zeta(L, m) = \frac{1}{\pi} \int_0^\infty \frac{dx}{\sqrt{m^2 L^2 + x^2}} \frac{1}{e^{\sqrt{m^2 L^2 + x^2}} - 1}. \quad (2.19)$$

are due to a mismatch between the normal ordering counterterms needed to define the ϕ^4 operator in infinite space and on the circle. One of them contributes to the vacuum energy density, and the other is a correction proportional to the mass operator V_2 :

$$V_2(L, m) = \sum_k \frac{1}{2\omega_k} (a_k a_{-k} + a_k^\dagger a_{-k}^\dagger + 2a_k^\dagger a_k). \quad (2.20)$$

In [1] we worked at circle sizes up to $L = 10m^{-1}$, and it was justified to neglect the exponentially small terms proportional to E_0 and z . Here, in some cases, we will work at smaller circle sizes. In this paper we will always keep these terms, which is actually straightforward in our algorithm.

The Hilbert space \mathcal{H} of the theory is the Fock space of the ladder eigenstates. As in [1], we will restrict our attention to the subsector of the Hilbert space consisting of the states of zero total momentum $P = 0$ and of the positive spatial parity $\mathbb{P} = 1$. The Hamiltonian (2.14) does not mix states of positive and negative field parity $\mathbb{Z}_2 : \phi \rightarrow -\phi$ (i.e. the states containing an even and odd number of particles). Thus the \mathbb{Z}_2 -even and \mathbb{Z}_2 -odd sectors can be studied separately. We will study both of them. Finally, we will truncate the Hilbert space to the subspace of states $\mathcal{H}(E_{\max})$ which have H_0 energy below a certain cutoff E_{\max} . Typically, we choose our cutoff so that the dimension of $\mathcal{H}(E_{\max})$ is ~ 10000 per \mathbb{Z}_2 sector. The Hamiltonian $H(L)$ restricted to the truncated Hilbert space is called the truncated Hamiltonian $H(L)_{\text{trunc}}$.

We evaluate the matrix elements of H_{trunc} , and the eigenvalues of the resulting finite matrix are then computed numerically. This gives what in [1] is called ‘‘raw’’ spectrum. It converges to the true nonperturbative spectrum with a rate which asymptotically goes as $1/E_{\max}^2$.

Convergence of the method can be improved by renormalizing the couplings. We refer the reader to [1] for a detailed explanation of the renormalization procedure.⁴ In the present work we will use an identical procedure, apart from a technicality that we now explain.

⁴Similar renormalization procedures were developed in the Truncated Conformal Space Approach literature [18–21]. The concrete version used by us shares a lot in common with the one in [22]; the small differences that exist were stressed in [1].

In [1], the leading renormalization coefficients were calculated by extracting the leading non-analytic behavior for $\tau \rightarrow 0$ of the quantities

$$I_k(\tau) = \int_{-L/2}^{L/2} dz G_L(z, \tau)^k, \quad (2.21)$$

where $G_L(z, \tau)$ is the two point function in finite volume, which can be expressed through periodization via the two point function in infinite volume:

$$G_L(z, \tau) = \sum_{n \in \mathbb{Z}} G(\sqrt{(z + nL)^2 + \tau^2}), \quad (2.22)$$

$$G(\rho) \equiv \frac{1}{2\pi} K_0(m\rho), \quad \rho \equiv \sqrt{z^2 + \tau^2}. \quad (2.23)$$

Here $K_0(m\rho)$ is a modified Bessel function of the second kind. Since $G(\rho)$ is exponentially suppressed for $m\rho \gg 1$, the contributions from $n \neq 0$ in (2.22) can be neglected as long as $mL \gg 1$. This is what we did in [1]. However in the present work we will encounter also the situation $mL = O(1)$. Our procedure will be to approximate:

$$G_L(z, \tau) \simeq G(\rho) + 2 \sum_{n=1}^{\infty} G(nL), \quad (2.24)$$

which simply adds a constant to the infinite-volume two point function. This approximation is justified because the higher order Taylor expansion terms of $G(\rho)$ around $\rho = nL$ would result in renormalization terms suppressed by powers of $m^2/E_{\max}^2 \ll 1$. The short-distance asymptotics of G_L used to calculate (2.21) is modified as (cf. (3.23) in [1]):

$$G_L(z, \tau) \approx -\frac{1}{2\pi} \log \left(\frac{e^\gamma}{2} m' \rho \right), \quad m' \equiv m \exp \left[-4\pi \sum_{n=1}^{\infty} G(nL) \right]. \quad (2.25)$$

It is then straightforward to generalize the renormalization procedure of [1] to the case $mL = O(1)$. E.g. the Hamiltonian renormalized by local counterterms is given by:

$$H(L)_{\text{ren}} = H_{\text{trunc}}(L) + \int dx N_m (\kappa_0 + \kappa_2 \phi^2 + \kappa_4 \phi^4), \quad (2.26)$$

where κ_i are given in [1], (3.34) where one has to put $g_4 = g$, $g_2 = 6z(L)g$, and replace $m \rightarrow m'$ in the expressions for the μ -functions in [1], (3.31). This Hamiltonian allows to calculate the spectrum with the convergence rate of $1/E_{\max}^3$. In the numerical computations in section 2.3.3 we will also include subleading, non-local corrections improving the convergence rate up to $1/E_{\max}^4$, for which we refer the reader to [1].

2.3.2 Dual theory

The Hamiltonian for the dual theory in finite volume is easiest derived as follows. Let us rewrite H' in (2.9) by adding and subtracting $\frac{1}{2}M^2\phi^2$:

$$H' = \int dx N_M \left(\frac{1}{2} \dot{\phi}^2 + \frac{1}{2} \phi'^2 + \frac{1}{2} M^2 \phi^2 \right) + N_M \left(-\frac{3}{4} M^2 \phi^2 + g \phi^4 + \Lambda \right). \quad (2.27)$$

This looks like the direct Hamiltonian with $m \rightarrow M$ and an extra negative mass squared perturbation. The passage to a finite volume is then analogous to the direct theory. We get

$$H'(L) = H_0 + \left[-\frac{3}{4}M^2 + 6\zeta g\right]V_2 + gV_4 + h, \quad (2.28)$$

$$h = \Lambda L + E_0 + 3\zeta^2 gL - \frac{3}{4}M^2\zeta L. \quad (2.29)$$

The building blocks have the same meaning as in section 2.3.1, except that we have to use M instead of m in all expressions: $H_0 = H_0(L, M)$, $\zeta = \zeta(L, M)$, etc.

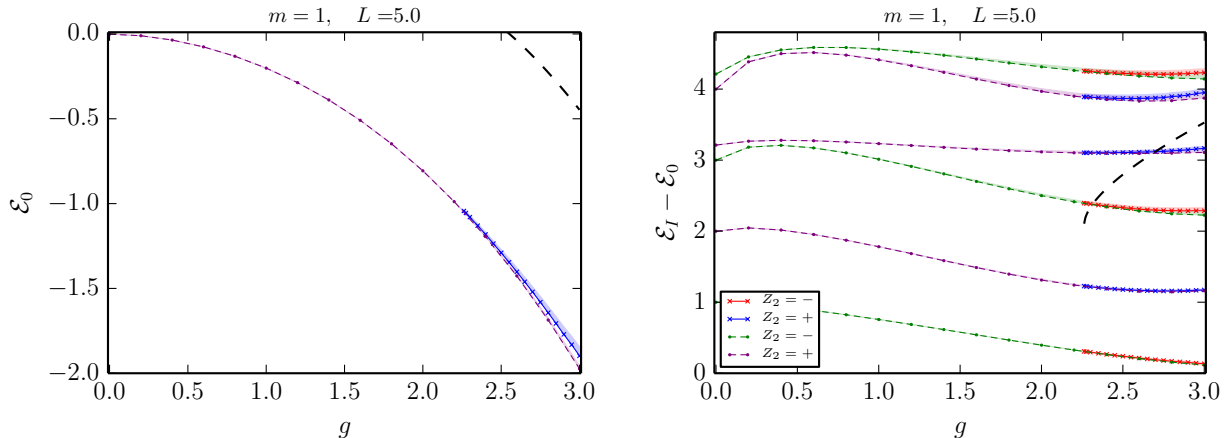


Figure 2: The ground state energy (left) and the spectrum of excitations (right) for the direct and the dual theory as a function of g for $m = 1$, $L = 5$. The excitation plot shows the energies of the \mathbb{Z}_2 odd and \mathbb{Z}_2 even energy levels. See the text for the details.

2.3.3 Comparison

In figure 2 we show the ground state energy \mathcal{E}_0 and the spectrum of excitations $\mathcal{E}_I - \mathcal{E}_0$ for $m = 1$, $L = 5$. We plot them as a function of the direct coupling $g = 0 - 3$. The results for the direct theory are given in the full range of g , whereas for the dual theory only for $g \geq g_c \approx 2.26$, where the dual description exists. As in [1], the error (shaded region) is estimated as the variation of the results upon using the “local” and “subleading” renormalization prescriptions.

We see that in the overlapping region the numerical predictions from the two descriptions agree very well. This is an explicit check of the Chang duality. This check is non-trivial, as in both descriptions the Hamiltonian is strongly coupled. To illustrate this, the black dashed lines in the plots represent the tree-level prediction for the vacuum energy and the lightest excitation in the dual description.

Computational details: The computation in the direct theory is carried out as described in section 2.3.1. The dual mass M for a given $g \geq g_c$ is determined by solving Eq. (2.4) numerically. We use the solution with the smaller X (and thus the larger M). The computation in the dual theory is then done using the Hamiltonian (2.28) with two couplings $g_2 = -\frac{3}{4}M^2 + 6z(L)g$ and

$g_4 = g$, i.e. by including $-\frac{3}{4}M^2$ into the perturbation. The renormalization procedure in [1] is applicable for such a general perturbation. It's not a problem for the method that g_2 is negative and comparable in size to the positive mass square term in H_0 . There is in fact a great deal of arbitrariness in how to split the ϕ^2 coefficient between the zeroth-order Hamiltonian and the perturbation. What we do here is just the fastest possibility, which turns out sufficient for the purposes of this section. More sophisticated ways of dealing with the dual theory will be developed in section 3.

3 The \mathbb{Z}_2 -broken phase

In section 2 we reviewed the Chang duality and tested it numerically in the strongly coupled region by comparing the results obtained from the dual and the direct descriptions. We will now focus on the region $g/m^2 \gg g_*/m^2$, where the theory is in the \mathbb{Z}_2 -broken phase. In this range of couplings the direct description is very strongly coupled and it's difficult to achieve good numerical accuracy. On the other hand, the dual Hamiltonian becomes weakly coupled ($g/M^2 \ll 1$). Therefore, we will use the dual Hamiltonian (2.9) as the starting point for the numerical calculations. It will be convenient to replace the value of Λ given in (2.13) by $\Lambda = M^2/(64g)$, which corresponds to having zero classical vacuum energy density of the dual Hamiltonian.

3.1 Modified zero mode treatment

In 2.3.1 we reviewed the method of [1] which treats all field modes on equal footing. This method is adequate in the \mathbb{Z}_2 -unbroken phase and in the \mathbb{Z}_2 -broken phase in moderate volumes, as in section 2.3.3. However, it becomes inefficient in the \mathbb{Z}_2 -broken phase in large volume. The physical reason is that the zero mode has then very different dynamics from the rest of the modes, acquiring a VEV. It makes sense to take this into account, and to treat the zero mode separately from the rest. We will now explain how this can be done.

First of all we will rewrite (2.28) making explicit the dependence on the zero mode. We will revert for the zero mode from using the oscillators a_0, a_0^\dagger to the field variable

$$\phi_0 = (a_0 + a_0^\dagger)/\sqrt{2LM} \quad (3.1)$$

and the corresponding conjugate momentum π_0 :

$$\pi_0 = i(a_0^\dagger - a_0)\sqrt{LM/2}. \quad (3.2)$$

Denoting by bar (resp. hat) all quantities involving only the nonzero (zero) modes, we have

$$H_0 = \bar{H}_0 + \frac{:\pi_0^2:}{2L} + \frac{LM^2}{2}:\phi_0^2:, \quad (3.3)$$

$$V_2 = \bar{V}_2 + L:\phi_0^2:, \quad V_4 = \bar{V}_4 + 4\bar{V}_3\phi_0 + 6\bar{V}_2:\phi_0^2: + L:\phi_0^4:. \quad (3.4)$$

Gathering everything we get

$$H'(L) = \bar{H}_0 + \hat{H} + W, \quad (3.5)$$

where \hat{H} depends only on the zero mode:

$$\hat{H} \equiv \frac{:\pi_0^2:}{2L} + L \left[-\frac{1}{4}M^2 + 6\zeta g \right] : \phi_0^2 : + Lg : \phi_0^4 : + h, \quad (3.6)$$

while W involves the interactions between the zero and the nonzero modes, and among the latter:

$$W \equiv \left[6g : \phi_0^2 : - \frac{3}{4}M^2 + 6\zeta g \right] \bar{V}_2 + 4g\phi_0 \bar{V}_3 + g\bar{V}_4. \quad (3.7)$$

In a large volume and for $g \ll M^2$, the quantum mechanics of (3.6) predicts that the wavefunction of ϕ_0 is peaked around the minima of the potential at $\phi_0^2 \approx M^2/(8g)$, with a width scaling asymptotically as $\langle (\Delta\phi_0)^2 \rangle \sim 1/(LM)$. For this ϕ_0 the coefficient of \bar{V}_2 in W vanishes. Intuitively this implies that, up to small perturbative corrections induced by the \bar{V}_3 and \bar{V}_4 terms, the nonzero modes of the field will stay in their vacuum state. This is true in a very large volume, and it provides a good starting point for a quantitative description in finite volume.

The idea of the method will be therefore to first solve the quantum mechanics of the zero modes, by neglecting its interaction with the nonzero modes. Having done so, the full Hamiltonian will be diagonalized in a Hilbert space whose basis wavefunctions are products of the exact zero mode wavefunctions and the harmonic oscillator wavefunctions for the nonzero modes. This is expected to be more efficient than the original method which would use harmonic oscillator wavefunctions also for the zero mode.

Concretely, the procedure goes as follows. The full Hilbert space can be written as a direct product:

$$\mathcal{H} = \hat{\mathcal{H}} \otimes \bar{\mathcal{H}}, \quad (3.8)$$

where $\hat{\mathcal{H}}$ and $\bar{\mathcal{H}}$ are the Hilbert spaces of the zero modes and nonzero modes, respectively. The truncated Hilbert space is then (l for low)

$$\mathcal{H}_l = \hat{\mathcal{H}}_l \otimes \bar{\mathcal{H}}_l, \quad (3.9)$$

where the basis of $\bar{\mathcal{H}}_l$ is formed by the harmonic oscillator states for the nonzero modes with energy $\bar{E} \leq \bar{E}_{\max}$, while $\hat{\mathcal{H}}_l$ is spanned by the first few low-lying eigenfunctions of \hat{H} :

$$\hat{H}|\psi_\alpha\rangle = \hat{\mathcal{E}}_\alpha|\psi_\alpha\rangle, \quad \alpha = 1 \dots s. \quad (3.10)$$

In practice, it will be sufficient to fix $s = 4$ or 5 .

A separate computation has to be done to find the $|\psi_\alpha\rangle$. We do this using the standard Rayleigh-Ritz method, working in the S -dimensional subspace of $\hat{\mathcal{H}}$ spanned by the original harmonic oscillator wavefunctions $(a_0^\dagger)^i|0\rangle$, $i = 0 \dots S-1$. The parameter $S \gg s$ can be chosen so large that the numerical error accumulated in this step is insignificant; in practice we choose $S = 500$. The eigenstates $|\psi_\alpha\rangle$ are thus found expanding them in the harmonic oscillator wavefunctions. This facilitates the subsequent computations of the matrix elements involving these states.

One can now compute the matrix elements of $H'(L)$ in the truncated Hilbert space and diagonalize it, finding the “raw” spectrum. As usual, we will employ a renormalization procedure to improve the precision. The necessary modifications are described in appendix A.

Comparison with prior work: The \mathbb{Z}_2 -broken phase of the ϕ^4 model has been previously studied via a Hamiltonian truncation method in Ref. [3]. There are many similarities between our works, and some differences. The main difference lies in the treatment of the zero mode (see also the discussion in [1], section 4.5). Ref. [3] compactifies the zero mode on a circle of large radius, and uses plane waves on this target space circle as the basis of trial wavefunctions. Instead, we resolve the zero mode dynamics and pick trial wavefunctions adapted to the quartic potential. Another difference is that they use conformal, massless, basis for the nonzero modes, while we use a massive basis. Matrix elements are easier to compute in the conformal basis, while a massive basis gives, we believe, a better initial approximation.

Notice that Ref. [3] uses a different parametrization of the Hamiltonian, corresponding to a different normal-ordering prescription. Translation to our parametrization will be given in section 3.3.3.

3.2 Varying the normal-ordering mass

It turns out that in the regime we will be considering, the most important term inducing the interactions between $\hat{\mathcal{H}}_l$ and $\bar{\mathcal{H}}_l$ is the \bar{V}_2 term in (3.7). This is because for the volumes that we will be able to consider, the localization of the ϕ_0 wavefunctions near the potential minimum is not very sharp, and the coefficient of \bar{V}_2 , viewed as a matrix in the space of the ϕ_0 eigenstates, has significant matrix elements. The \bar{V}_3 and \bar{V}_4 terms will be suppressed at weak coupling.

Empirically, we concluded that the one-loop renormalization procedure, including the modifications to be described in appendix A, is insufficient to fully describe the truncation effects arising from the big \bar{V}_2 term. Moreover, estimating the accuracy as the difference between the “local” and “subleading” renormalized answers was found inadequate in such a situation. Notice that the V_2 term renormalizes at quadratic order only the unit operator coefficient and this correction does not affect the spectrum of excitations [22, 1] (this statement remains approximately true in the scheme with the separated zero mode discussed here). Ideally, to estimate the error one would have to compute the renormalization effects of cubic order in the problematic operator. Here we will resort to an interim alternative technique, which we now describe.⁵

In the modified method as described in the previous section, the trial wavefunctions of the nonzero modes are taken to be those of the free massive boson of mass M , i.e. the bare mass appearing in the Lagrangian. We will now consider the formalism in which one can vary the mass parameter μ of the trial wavefunctions. As in [14], this will then be used to control the accuracy of our computations, since the exact spectrum should be independent of μ . Apart from the accuracy issues, varying μ is also natural from the point of view of searching for an optimal zeroth order approximation to the ground state, in the spirit of variational methods.

⁵Another interesting possibility is to incorporate the coefficient of \bar{V}_2 into the mass of nonzero modes, making it ϕ_0 -dependent. This creates technical difficulties of its own and was not tried in this work.

So we rewrite the infinite-volume Hamiltonian (2.27) by using the Coleman relations (2.10):

$$H' = \int dx N_\mu \left(\frac{1}{2} \dot{\phi}^2 + \frac{1}{2} \phi'^2 + \left(-\frac{1}{4} M^2 + 6gZ \right) \phi^2 + g\phi^4 + \Lambda_\mu \right), \quad (3.11)$$

$$\Lambda_\mu = \Lambda - \frac{1}{4} M^2 Z + 3gZ^2 + Y, \quad (3.12)$$

where $Z = Z(M, \mu)$, $Y = Y(M, \mu)$ are defined in (2.11) with the replacement $M \rightarrow \mu, m \rightarrow M$. We then pass to finite volume as in section 2.3.2:

$$H'(L) = H_0 + \left[-\frac{1}{4} M^2 - \frac{1}{2} \mu^2 + 6(Z + \zeta)g \right] V_2 + gV_4 + h_\mu, \quad (3.13)$$

$$h_\mu = \Lambda_\mu L + E_0 + 3\zeta^2 gL + \left(-\frac{1}{4} M^2 - \frac{1}{2} \mu^2 + 6gZ \right) \zeta L. \quad (3.14)$$

where $H_0, V_2, V_4, E_0, \zeta$ are defined with respect to μ . Finally, we separate the zero mode as in section 3.1. The final Hamiltonian has the form (3.5) where $\bar{H}_0 = \bar{H}_0(L, \mu)$ while \hat{H} and W are given by:

$$\hat{H} = \frac{:\pi_0^2:}{2L} + L \left[-\frac{1}{4} M^2 + 6(Z + \zeta)g \right] : \phi_0^2 : + Lg : \phi_0^4 : + h_\mu, \quad (3.15)$$

$$W = \left[6g : \phi_0^2 : - \frac{1}{4} M^2 - \frac{1}{2} \mu^2 + 6(Z + \zeta)g \right] \bar{V}_2 + 4g\phi_0 \bar{V}_3 + g\bar{V}_4. \quad (3.16)$$

This is the Hamiltonian which we use for numerical calculations, varying μ in the range 0.9 - 1.1 M . This will give an idea of the systematic error due to the truncation.

3.3 Results

From previous estimates, we know that the critical point lies at $g/m^2 \approx 2.97(14)$ [1],⁶ which by making use of the Chang duality corresponds to $g/M^2 \approx 0.26$. Here we will limit ourselves to values $g/M^2 \leq 0.2$, as beyond this value it appears difficult to reach the limit $L \rightarrow \infty$ and get a stable spectrum. M will be set to 1 throughout this section, unless stated otherwise.

We are now going to present the results for the two sectors of excitations of the theory. First, we will discuss the perturbative sector, which in the $L \rightarrow \infty$ consists of two decoupled towers of excitations around the two vacua with the opposite-sign VEV for the field. We will then turn to the non-perturbative sector of “kink” states which have topological charge, interpolating between the two vacua. Given the periodic boundary conditions imposed in our method, the kink sector will be studied here only indirectly, through the splitting of quasi-degenerate perturbative states in finite volume.

3.3.1 Perturbative sector

In figure 3 we plot the ground state energy density and the low-energy excitation spectrum for $M = 1, L = 12$. For the ground state energy density we show both the “raw” and renormalized⁷ results,

⁶For more precise estimates by different methods see [9, 13, 10, 16].

⁷In this section only local renormalization, in terminology of [1], was used. Subleading nonlocal corrections were found to be totally negligible.

while for the spectrum only the renormalized results, because the raw/renormalized difference is negligible. As explained above, we don't think this difference gives a fair idea of the truncation error in the situation at hand. Instead, we estimate the error for the spectrum by varying the normal-ordering mass $\mu = 0.9 - 1.1$. In making these plots we fixed $s = 4$, while the cutoff \bar{E}_{\max} was chosen so that \mathcal{H}_l has dimension around 10000 – 15000. We checked that increasing s does not change the results significantly.

We see that the first excited level is almost degenerate with the ground state. The splittings for the higher-energy levels are larger. This is because for the higher energy states it's easier to tunnel through the potential barrier separating the two infinite-volume vacua, which has a finite height for a finite L .

In figure 4 we show the same plots for $L = 20$. One can see that the energy splitting reduces but the truncation error increases (as one has to reduce \bar{E}_{\max} in order to keep the total number of states the same).

Finally, in figure 5 we plot the vacuum energy density and the spectrum for $g = 0.1$ as a function of L . One can see how the renormalization procedure is effective for the vacuum energy density, as its renormalized value reaches a constant for sufficiently large L , while its “raw” values does not. In the spectrum also the physical mass reaches a constant as expected.

Notice that for sufficiently small g the interaction in the considered model is attractive (the cubic vertex squared attraction overcomes the quartic vertex repulsion) [23, 3]. Therefore the second energy level pair in the spectrum in figure 5 is expected to asymptote to $m_2 < 2m_{\text{ph}}$ (where m_{ph} is the single particle mass) as $L \rightarrow \infty$, i.e. it represents a bound state. The numerical results seem consistent with this expectation, although the precision is insufficient to extract m_2 accurately. In general, it is hard to extract the perturbative bound state mass from the infinite-volume limit, as the asymptotic convergence sets in at $L \approx (m_{\text{ph}}^2 - m_2^2/4)^{-1/2}$ [24], which diverges as $g \rightarrow 0$.

In Appendix B we compare the numerical results for Λ and m_{ph} with the predictions from perturbation theory, showing very good agreement at small couplings.

It is also interesting to analyze the higher-energy states in the spectrum. In figure 6 we redo the previous plot for $g = 0.05$, including a few more eigenvalues. Above the stable particle mass and the bound state, one can see the multiparticle states whose energy depends on L according to the dispersion relations in finite volume.⁸ Furthermore, the horizontal line with energy $\approx 2.5 < 3m_{\text{ph}}$ represents a resonance. Due to the non-integrability of the theory, that state is not stable, as its energy is larger than $2m_{\text{ph}}$. Indeed, the horizontal line does not cross the multiparticle states as could seem at first glance, thanks to the phenomenon of avoided crossing. See [25] for a discussion of how resonances should appear in the finite volume spectrum.

3.3.2 Non-perturbative sector

As already mentioned, in finite volume non-perturbative effects lift the spectrum degeneracy both for the ground state and for all the excited states. For small coupling, these effects can be

⁸See e.g. the discussion in [3], appendix B.

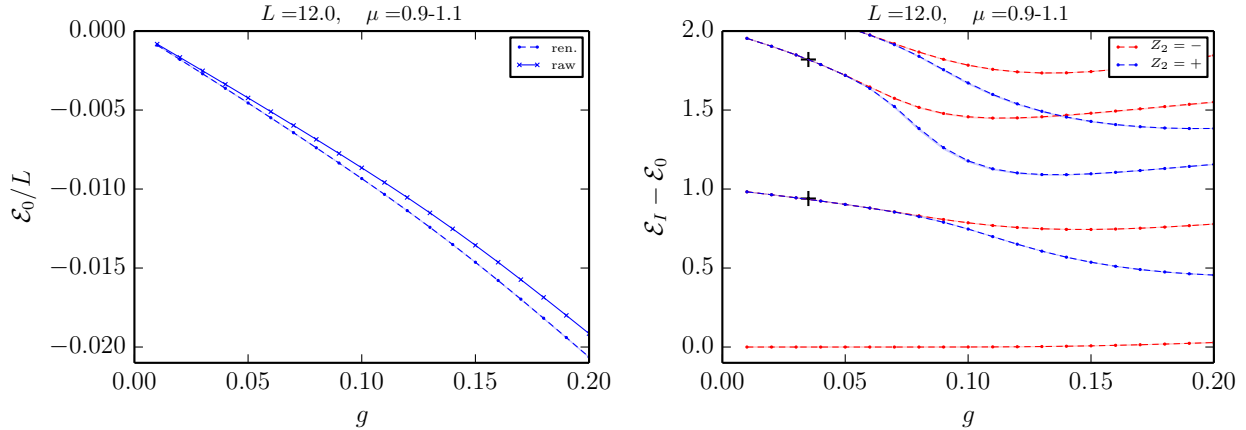


Figure 3: The ground state energy density and the low-energy excitation spectrum as a function of g for $L = 12$; see the text. Results extracted from [3] are shown by crosses (whose size does not reflect the uncertainty), see section 3.3.3.

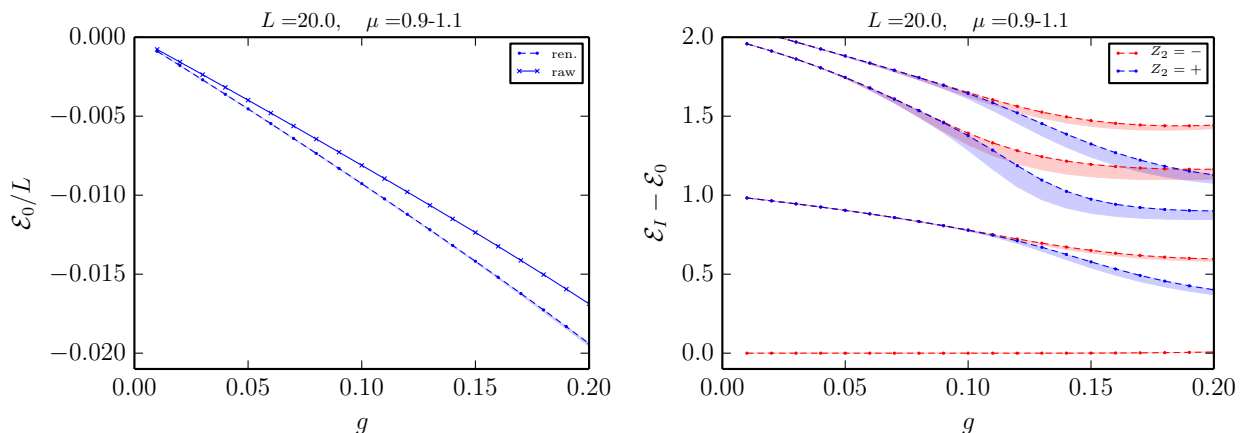


Figure 4: Same as in figure 4 but for $L = 20$.

interpreted as tunneling due to the semiclassical field configurations interpolating between the two vacua (“kinks”). The splitting depends on the mass of the kink. Here we will need the semiclassical prediction for the splitting of the first two energy levels (the ground state, which lives in the \mathbb{Z}_2 even sector, and the \mathbb{Z}_2 odd state just above it). Including the leading semiclassical results and the one-loop determinant fluctuations around it, the splitting for small g/M^2 is given by (see appendix C):

$$\Delta\mathcal{E} = \mathcal{E}_1 - \mathcal{E}_0 \approx \sqrt{\frac{M^3}{6\pi g L}} e^{-LM_{\text{kink}} - f(ML)}, \quad M_{\text{kink}} = \frac{M^3}{12g} + M \left(\frac{1}{4\sqrt{3}} - \frac{3}{2\pi} \right), \quad (3.17)$$

where M_{kink} is the kink mass in the one-loop approximation, first computed in [26]. Corrections are suppressed by g/M^2 and by $1/(LM_{\text{kink}})$. The function $f(x)$, given in (C.24), approaches zero

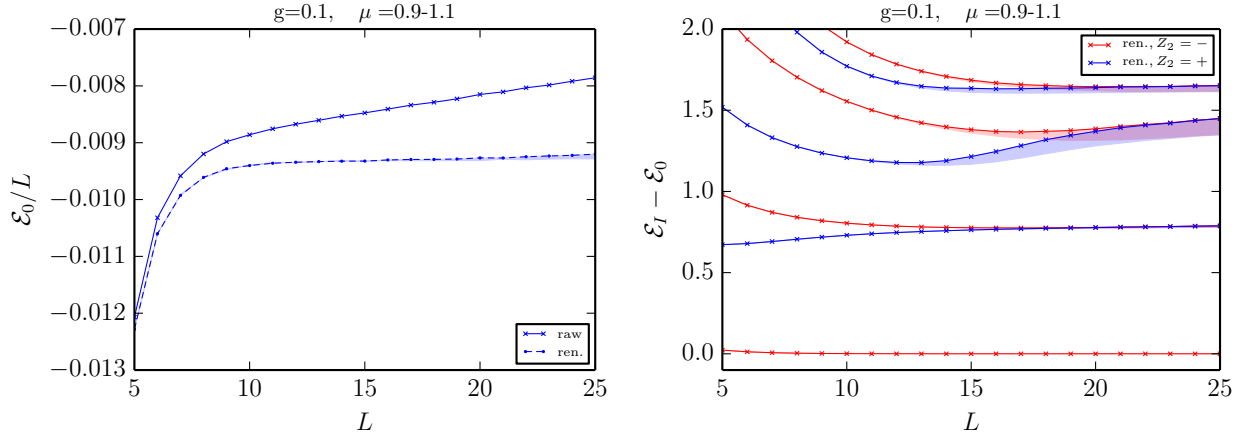


Figure 5: Results for $g = 0.1$ plotted as a function of L .

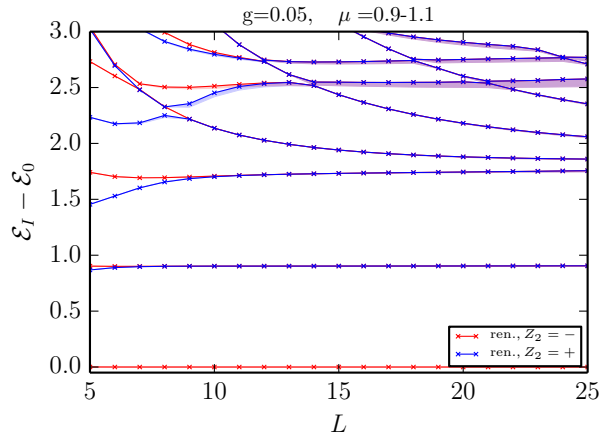


Figure 6: Same as in the right-hand figure 5 but for $g = 0.05$.

exponentially fast for $LM \gg 1$.

Our numerical method allows to extract $\Delta\mathcal{E}$ with high precision and to compare with this formula. In figure 7 we present as an example the renormalized numerical results⁹ for $M = 1$, $g = 0.05$. We used $s = 5$, checking that its increase does not change significantly the numerics, while \bar{E}_{\max} was fixed such as to have a basis dimension ~ 10000 for each L . We plot $\sqrt{L} e^{f(ML)} \Delta\mathcal{E}$ as a function of L in logarithmic scale in order to observe a linear trend, as expected from (3.17), and perform a fit in a region chosen by eye such that the data look close to a straight line:

$$\log[\sqrt{L} e^{f(ML)} \Delta\mathcal{E}] \approx \alpha - M_* L. \quad (3.18)$$

The value of L must be not too low so that the exponential law decay sets in, and not too high otherwise $\Delta\mathcal{E}$ becomes smaller than the precision of our method. We then compare the fitted values of α and M_* with the expectations from (3.17).

⁹The difference between “raw” and renormalized is negligible in the present analysis.

We carried out this analysis for several values of the coupling between 0.01 and 0.1, finding both α and M_* very close to the expected values. The comparison of M_* with M_{kink} is plotted in figure 8 as a function of g . It turns out that in the range of points where the fit is made $f(ML)$ is very small and does not influence the fit, except a little for the smallest considered values of g . On the other hand including \sqrt{L} is crucial for reaching the agreement. One can see that the accord with the semiclassical prediction M_{kink} (black line) is very good.

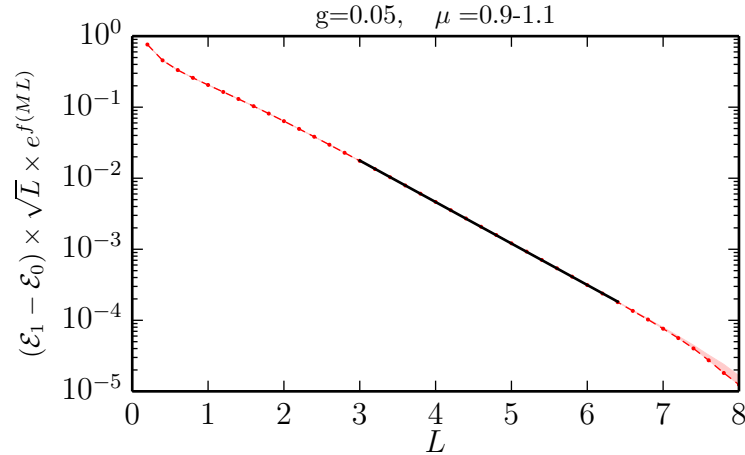


Figure 7: Ground state splitting as a function of L for $g = 0.05$; see the text.

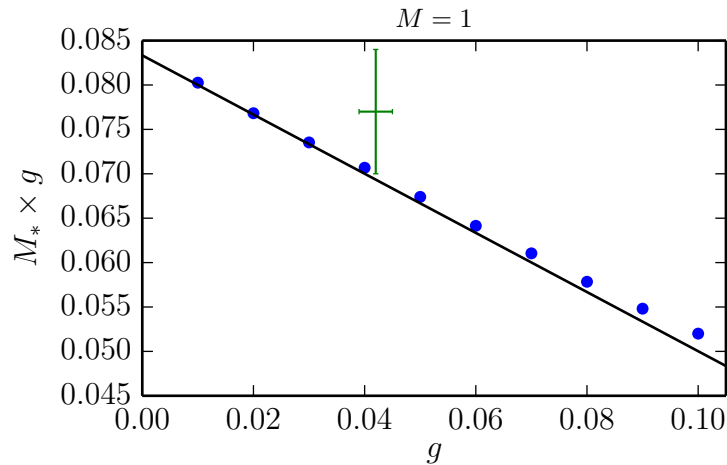


Figure 8: Comparison between the fitted and the theoretically predicted value of the kink mass; see the text. The green cross represents, with error bars, a result from [3] as discussed in section 3.3.3.

3.3.3 Comparison to Ref. [3]

For comparison we included in figures 3,8 a few data points extracted from [3]. Ref. [3] parametrizes the theory by two couplings G_2, G_4 which they denote g_2, g_4 ; we capitalized to avoid confusion with

our notation in other parts of this paper. Their couplings are not identical to ours; because of the different field normalization $g = 2\pi G_4$. More importantly, their ϕ^4 operator is normal-ordered differently, by subtracting the normal-ordering constants for all nonzero massless modes in finite volume $L(= \text{their } R)$. Going to our normal ordering prescription (in infinite volume),

$$:\phi^4:_{\text{their}} \rightarrow N_m(\phi^4) - C(mL)N_m(\phi^2) + \text{const.}, \quad C(mL) = -(3/\pi) \log[e^\gamma mL/(4\pi)], \quad (3.19)$$

where γ is the Euler-Mascheroni constant. We don't pay attention to the ground state energy renormalization here. To put their Hamiltonian into the canonical form (2.8) (resp. (2.9)) one has to solve the two equations

$$G_2 - 2gC(mL) = m^2 \quad (\text{resp. } G_2 - 2gC(ML) = -M^2/2) \quad (3.20)$$

for m or M respectively. Keeping $G_{2,4}$ fixed and varying L thus induces a logarithmic variation of the infinite-volume mass parameters. Although for the small quartic couplings considered in [3] this variation is not huge (order 10%), it may be problematic for extracting the spectrum by approaching the large L limit. It would seem more appropriate to vary G_2 with L while keeping m or M fixed.

The two data points (crosses) in figure 3 were extracted from figure 10(b,d) of [3], where $G_2 = -0.1$, $G_4 = 1.2 \times 10^{-3}$. This corresponds to $g/M^2 \approx 0.035$ at $ML = 12$. The agreement between their and our results is good. Their determination of the kink mass for the same $G_{2,4}$ is shown in figure 8. Here $g/M^2 = 0.042(3)$, varying within the range of L used in their fit. The large error bars on M_{kink} may be due to this variation. Also, they did not consider the pre-exponential factor in (3.17).

A remark is in order concerning the discussion in [27, 3], which views the particles in the topologically trivial sector as bound states of kinks. A semiclassical prediction is given for their masses ([3], (28)):

$$m_{\text{sc},n} = 2M_{\text{kink}} \sin(n\pi\xi/2), \quad n = 1 \dots [1/\xi], \quad (3.21)$$

where

$$\xi = M/(\pi M_{\text{kink}}) \quad (3.22)$$

in our notation. The lightest mass $m_{\text{sc},1}$ has to be identified with our m_{ph} , while the second $m_{\text{sc},2}$ with the bound state mass m_2 discussed in section 3.3.1. The other masses correspond not to stable particles but to resonances in a non-integrable theory like the one we are considering. The total number of particles is predicted to be $[1/\xi]$.

The semiclassical prediction is valid for $\xi \ll 1$, but if one could extrapolate it to $\xi = O(1)$ one would naively predict that for $\xi > 1$ the topologically trivial sector would be devoid of particles. This would be analogous to the phase of the sine-Gordon model for $4\pi < \beta^2 < 8\pi$. Of course it's far from clear if such an extrapolation is trustworthy.

From the kink mass formula (3.17) we have $\xi = 1$ for $g/M^2 \approx 0.12$, just outside the region that we explored, and well below the critical point at $g_c/M^2 \approx 0.26$. It will be interesting to study this range in the future. One minimalistic possibility is that the topologically trivial particles disappear only at the critical point. Indeed, its neighborhood is described by the thermally perturbed 2d Ising model CFT, which is free massive Majorana fermion theory. In the low-temperature phase,

the fermionic excitations are naturally identified with the kink states interpolating between the two vacua. There are no bound states since the fermions are free.¹⁰

4 Conclusions

In this paper we followed up on our earlier study [1] of the Hamiltonian truncation technique applied to the ϕ^4 theory in two dimensions. The main results derived in this work can be summarized as follows:

- According to an exact duality, reviewed in section 2, the theory under consideration can be expressed via two different Lagrangian formulations. We proved that, even at strong coupling, the Hamiltonian truncation method correctly predicts the same low-energy spectrum of excitations in the two cases, despite the fact that they look totally different at the zeroth order. We regard this as a non-trivial check of the method.
- We showed how to modify the method in order to improve its accuracy in the spontaneously broken phase. We found very good agreement with the predictions from perturbation theory and semiclassics in the perturbative and non-perturbative sectors. To approach the critical region as in [1] will require further improvements of the method.¹¹

We continue to believe that the potential of “exact diagonalization” techniques, among which we have implemented a particular realization in the present work, is very large and has to be explored further. Some other representative applications to non-integrable theories to be found in the literature are [25, 30–32, 3, 33–36] in $d = 2$. In $d > 2$ the only work is [22].

In the future it would be interesting to extend the present analysis, for instance by studying the topological spectrum of kink-states directly,¹² or consider more complicated theories involving scalar-fermion interactions, which should not be too technically challenging.¹³ In the long term, in order to solve numerically higher dimensional theories, it will be necessary at the very least to refine the renormalization technique, as the RG flow becomes more weakly relevant.¹⁴ The hope is that exact diagonalization techniques can evolve into computationally efficient tools to address difficult problems in quantum field theory.

¹⁰**Note added:** This ‘minimalistic possibility’ can now be ruled out, in favor of the original scenario of [27], based on the very recent results of [28]. As this paper shows, the second lightest particle m_2 in the topologically trivial spectrum becomes unstable with respect to decay into two kinks for $g/M^2 \gtrsim 0.075$, while for the lightest particle m_{ph} this happens for $g/M^2 \gtrsim 0.125$. The possibility of the first of these decays could be observed already from our mass plots in Figs. 4,8.

¹¹**Note added:** Rapid progress in this direction should be possible thanks to the technical and conceptual improvements discussed in [28, 29], which appeared a few weeks after our work.

¹²**Note added:** This has just been achieved in [28]. The authors use a different truncation scheme and diagonalization routine, and they are able to calculate the kink mass up to $g \sim 0.2$ (in our conventions).

¹³See [37] for early work.

¹⁴**Note added:** See [29] for recent progress towards the calculation of higher order renormalization coefficients.

Acknowledgements

We are grateful to Giuseppe Mussardo for the comments of the draft. This research was partly supported by the National Centre of Competence in Research SwissMAP, funded by the Swiss National Science Foundation. The work of L.V. is supported by the Swiss National Science Foundation under grant 200020-150060.

A Renormalization in the \mathbb{Z}_2 -broken phase

We invite the reader to go first through the explanation of the renormalization procedures for the \mathbb{Z}_2 -symmetric phase presented in detail in [1], as the notation and logic below are closely inherited from that discussion.

Let us start from the full eigenvalue problem:

$$H.c = \mathcal{E}c. \quad (\text{A.1})$$

The full Hilbert space can be split into “low” energy and “high” energy subspaces:

$$H_l = \hat{\mathcal{H}}_l \otimes \bar{\mathcal{H}}_l, \quad (\text{A.2})$$

$$H_h = (\hat{\mathcal{H}}_h \otimes \bar{\mathcal{H}}_l) \oplus (\hat{\mathcal{H}}_l \otimes \bar{\mathcal{H}}_h) \oplus (\hat{\mathcal{H}}_h \otimes \bar{\mathcal{H}}_h). \quad (\text{A.3})$$

Accordingly, (A.1) can be projected onto these subspaces:

$$H_{ll}.c_l + H_{lh}.c_h = \mathcal{E}c_l, \quad (\text{A.4})$$

$$H_{hl}.c_l + H_{hh}.c_h = \mathcal{E}c_h. \quad (\text{A.5})$$

“Integrating out” c_h via the second equation, we get:

$$(H_{ll} + \Delta H)c_l = \mathcal{E}c_l, \quad (\text{A.6})$$

$$\Delta H = -H_{lh} \frac{1}{H_{hh} - \mathcal{E}} H_{hl} = -W_{lh} \frac{1}{H_{hh} - \mathcal{E}} W_{hl}, \quad (\text{A.7})$$

where we used that in the Hamiltonian (3.5) only W will mix the low and high subspaces. At leading order one can neglect W in the denominator, which gives:

$$\Delta H \approx -W_{lh} \frac{1}{\hat{H} + \bar{H}_0 - \mathcal{E}} W_{hl} = - \sum_{i \in \mathcal{H}_h} \frac{1}{E_i - \mathcal{E}} P_l W |i\rangle \langle i| W P_l \quad (\text{A.8})$$

where a summation over all the states in \mathcal{H}_h appears.

It turns out that the effect induced by the truncation of $\hat{\mathcal{H}}$ is less significant than for $\bar{\mathcal{H}}$. It’s also less expensive to control. We found that fixing the corresponding cutoff s to 4 or 5 basically stabilizes the results. For this reason we will only take into account the renormalization effect

coming from the nonzero field modes. This means that we will restrict the sum in (A.8) to go only over the $\hat{\mathcal{H}}_l \otimes \bar{\mathcal{H}}_h$ part of \mathcal{H}_h . Therefore, we approximate:

$$\Delta H \approx - \sum_{\psi_\alpha \in \hat{\mathcal{H}}_l} \sum_{k \in \bar{\mathcal{H}}_h} \frac{1}{\hat{\mathcal{E}}_\alpha + \bar{E}_k - \mathcal{E}} W |\psi_\alpha, k\rangle \langle \psi_\alpha, k| W \quad (\text{A.9})$$

where we dropped the projectors P_l to avoid cluttering. The potential matrix W can be schematically written as:

$$W = \sum_{a=2,3,4} \hat{m}_a \otimes \bar{V}_a, \quad (\text{A.10})$$

where \hat{m}_a and \bar{V}_a are matrices in the $\hat{\mathcal{H}}$ and $\bar{\mathcal{H}}$, respectively. Therefore:

$$\Delta H \approx - \sum_{a,b} \sum_{\psi_\alpha \in \hat{\mathcal{H}}_l} \left(\hat{m}_a |\psi_\alpha\rangle \langle \psi_\alpha| \hat{m}_b \right) \otimes \left(\sum_{k \in \bar{\mathcal{H}}_h} \frac{1}{\hat{\mathcal{E}}_\alpha + \bar{E}_k - \mathcal{E}} \bar{V}_a |k\rangle \langle k| \bar{V}_b \right). \quad (\text{A.11})$$

The matrix elements $\left(\hat{m}_a |\psi_\alpha\rangle \langle \psi_\alpha| \hat{m}_b \right)$ can be computed explicitly, while the second factor in (A.11) is evaluated with the same technique developed in [1]:

$$\sum_{k \in \bar{\mathcal{H}}_h} \frac{1}{\hat{\mathcal{E}}_\alpha + \bar{E}_k - \mathcal{E}} \bar{V}_a |k\rangle \langle k| \bar{V}_b = \int_{\bar{E}_{\max}}^{\infty} dE \frac{1}{\hat{\mathcal{E}}_\alpha + E - \mathcal{E}} M^{ab}(E), \quad (\text{A.12})$$

$$M^{ab}(E)_{ij} dE \equiv \sum_{k: E \leq \bar{E}_k \leq E+dE} (\bar{V}_a)_{ik} (\bar{V}_b)_{kj}, \quad (\text{A.13})$$

where the matrix elements M_{ij}^{ab} can be related to the non-analytic behavior of two-point functions of the potential operators:

$$C^{ab}(\tau)_{ij} = \langle i | \bar{V}_a(\tau/2) \bar{V}_b(-\tau/2) | j \rangle = \int_0^{\infty} e^{-[E - (E_i + E_j)/2]} M_{ij}^{ab}(E), \quad (\text{A.14})$$

$$\bar{V}_a(\tau) \equiv e^{H_0 \tau} \bar{V}_a e^{-H_0 \tau}. \quad (\text{A.15})$$

The quantities $C^{ab}(\tau)_{ij}$ are computed as in [1] using the Wick theorem. The only difference is that the boson two point function $\bar{G}(\rho)$ in the present case does not include the contribution from the zero mode:

$$\bar{G}(\rho) = G(\rho) - \frac{1}{2LM}. \quad (\text{A.16})$$

B Perturbation theory checks

We computed the first few perturbative corrections to the ground state energy density Λ and the physical particle mass m_{ph} for the potential density:

$$\mathcal{V} = \frac{1}{2} M^2 N_M(\phi^2) + g_3 N_M(\phi^3) + g_4 N_M(\phi^4) \quad (\text{B.1})$$

The symmetric double-well case of Eq. (2.3) can be recovered by setting $g_4 = g$, $g_3 = \sqrt{2g_4}M$, but we will keep the couplings independent for the sake of generality.

For comparison with numerics, we will need results for $\Delta m^2 = m_{\text{ph}}^2 - M^2$ and Λ up to the second order in g . In terms of g_3, g_4 , we need to include all diagrams up to order $O(g_4^2)$, $O(g_3^2)$, $O(g_3^2 g_4)$ and $O(g_3^4)$. The results are¹⁵ ($\bar{g}_3 \equiv g_3/M^2$, $\bar{g}_4 \equiv g_4/M^2$):

$$\begin{aligned} \Lambda/M^2 &= \text{[diagram 1]} + \text{[diagram 2]} + \text{[diagram 3]} + \text{[diagram 4]} + \text{[diagram 5]} + \dots \\ &= -0.0445289\bar{g}_3^2 - \frac{21\zeta(3)}{16\pi^3}\bar{g}_4^2 - (0.0109030(51) + 0.026854(32))\bar{g}_3^4 + 0.0799586(41)\bar{g}_3^2\bar{g}_4 + \dots \end{aligned} \quad (\text{B.2})$$

and

$$\begin{aligned} \Delta m^2/M^2 &= \text{[diagram 1]} + \text{[diagram 2]} + \text{[diagram 3]} + \text{[diagram 4]} \\ &\quad + \text{[diagram 5]} + \text{[diagram 6]} + \text{[diagram 7]} + \dots \\ &= -\sqrt{3}\bar{g}_3^2 - 1.5\bar{g}_4^2 - (2.2492(37) + 2.8020(70))\bar{g}_3^4 \\ &\quad + (1.06864(15) + 1.9998(10) + 5.50025(91))\bar{g}_3^2\bar{g}_4 + \dots \end{aligned} \quad (\text{B.3})$$

In figure 9 we compare the above predictions for $g_4 = g$, $g_3 = \sqrt{2g_4}M$ with the numerical spectra obtained with our method for $M = 1$, $L = 12$. We use the zero-mode cutoff $s = 4$ and adjust \bar{E}_{max} so that the basis dimension is ~ 10000 in each sector.

In the left plot we show the renormalized results for Δm^2 , computed both in the \mathbb{Z}_2 -even and \mathbb{Z}_2 -odd spectra, with an error estimate given by variation of the normal ordering mass. We observe a reasonably good agreement for $g \lesssim 0.04$.¹⁶ For larger g , the deviation may be attributed to higher-order perturbative effects and to the finite-volume splitting affecting the numerics.

In the right plot we show instead both the “raw” and renormalized results for the ground state energy density, extracted from both \mathbb{Z}_2 -even and \mathbb{Z}_2 -odd spectra. Again, an error estimate for the renormalized values is attributed by varying the normal ordering mass. We see a perfect agreement with the perturbative prediction until the finite-volume splitting between the eigenvalues kicks in.

Note added (April 2019) Eq. (B.3) contains several mistakes. First, errors from Monte Carlo integration in diagrams of order g_3^4 and $g_3^2 g_4$ are underestimated. Second, we missed two tadpole diagrams (one at order g_3^4 and one at order $g_3^2 g_4$). Third, the correct formula should include wavefunction-renormalization effects, which at the given order come from the p^2 dependence of the first diagram in (B.3) and further correct the g_3^4 coefficient. Taking into account all these effects, and substituting $g_3 = \sqrt{2g_4}$, the correct formula for the mass correction is (see [38], Eq. (4.12))

¹⁵We do not report explicitly the symmetry factors for the diagrams. Most of them were evaluated numerically by Monte Carlo integration using coordinate space propagators. We did not invest much effort in analytic results.

¹⁶We haven’t investigated the reasons behind a small residual deviation visible in this region. One possible reason is that we may be underestimating the renormalization corrections by including contributions only from the $\hat{\mathcal{H}}_l \otimes \bar{\mathcal{H}}_h$ part of the high energy Hilbert space. See appendix A.

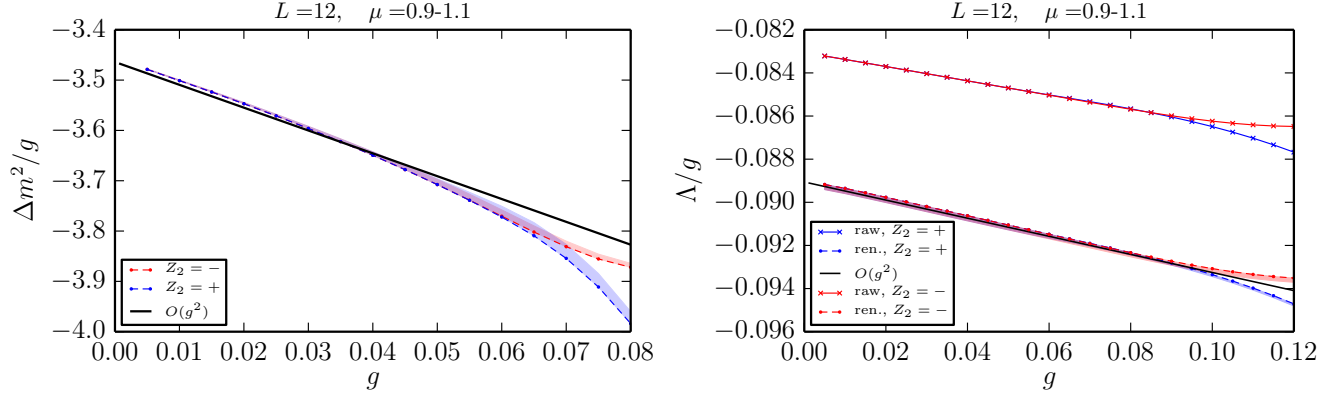


Figure 9: Comparing perturbative and numerical predictions; see the text.

$\Delta m^2/M^2 = -2\sqrt{3}g_4 - 4.1529(18)g_4^2 + \dots$. With this formula, the left plot in Fig.9 is replaced by Fig.10. We thank Gabriele Spada for pointing out that we missed the tadpole diagrams.

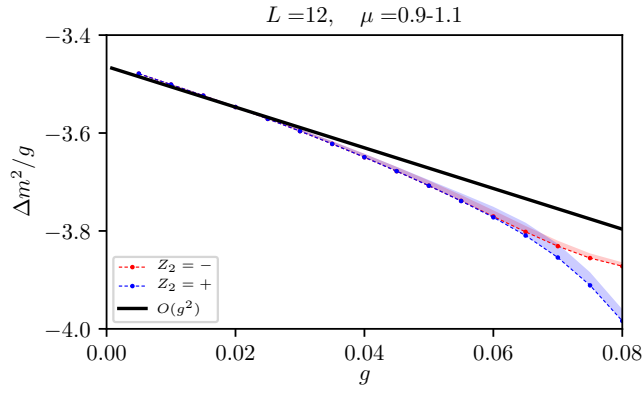


Figure 10: Comparing perturbative and numerical predictions for the mass gap, with corrected perturbative coefficients; see the text.

C Ground state splitting

We will review here the derivation of Eq. (3.17).¹⁷ We start from the Euclidean action:

$$S = \int d^2x \left[\frac{1}{2}(\partial\phi)^2 + g(\phi^2 - c^2)^2 \right], \quad (\text{C.1})$$

¹⁷See [39] for a pedagogical discussion in quantum mechanics, and [40] for an analogous computation for the partition function at finite temperature, which can be interpreted as a computation of the coefficient κ in (C.10).

which entails the perturbative particle mass $m^2 = 8gc^2$. The normal ordering prescription for renormalization adopted in this work is equivalent to the mass renormalization:¹⁸

$$S \rightarrow S - \frac{\delta m^2}{4} \int d^2x \phi^2, \quad \delta m^2 = \frac{6g}{\pi} \int_{-\infty}^{\infty} dk \frac{1}{\sqrt{k^2 + m^2}}. \quad (\text{C.2})$$

We will compute the matrix elements:

$$\mathcal{A}_{\pm} = \langle \phi = \pm c | e^{-H\tau_0} | \phi = c \rangle = \mathcal{N} \int \mathcal{D}\phi e^{-S[\phi]}, \quad (\text{C.3})$$

where the path integral in the r.h.s. is defined with the boundary conditions $\phi(x, \tau_0/2) = \pm c$, $\phi(x, -\tau_0/2) = c$. The path integral measure normalization factor \mathcal{N} will be fixed below. The results for the matrix elements will then be translated into the energy splitting.

Consider first the transition amplitude from c to $-c$ in the one-instanton approximation. The instanton takes the form:

$$\phi_0(x, \tau) = c \tanh \frac{m(\tau - \tau_c)}{2}, \quad (\text{C.4})$$

where the center τ_c is arbitrary. This solution has action:

$$S_0 + \delta S_0 = L \frac{m^3}{12g} - L \delta m^2 \frac{c^2}{4} \int_{-\infty}^{\infty} d\tau \left(\tanh^2 \frac{m\tau}{2} - 1 \right) = L \frac{m^3}{12g} + L \frac{\delta m^2}{8g} m, \quad (\text{C.5})$$

where we included the contribution due to the mass counterterm. We need $S_0 \gg 1$ for the validity of the semiclassical approximation.

At the one-loop order, (C.3) can be approximated by:

$$\mathcal{N} \int \mathcal{D}\phi e^{-S[\phi]} \approx e^{-S_0} \mathcal{N} \int \mathcal{D}\eta e^{-\int \eta \frac{\delta^2 S}{\delta \phi^2} \eta}. \quad (\text{C.6})$$

Taking into account the presence of the zero mode of the quadratic fluctuation operator $\frac{\delta^2 S}{\delta \phi^2}$ due to the invariance of S under a shift of τ_c , this results in:

$$\sqrt{\frac{S_0}{2\pi}} e^{-S_0} \mathcal{N} [\det'(-\square + V'')]^{-1/2} \tau_0, \quad (\text{C.7})$$

where the prime indicates that the zero mode has been removed from the determinant, and we replaced the integral over the zero mode with [39]:

$$\int dc_0 = \sqrt{\frac{S_0}{2\pi}} \int_{-\tau_0/2}^{\tau_0/2} d\tau. \quad (\text{C.8})$$

To fix \mathcal{N} , consider the $0 \rightarrow 0$ transition amplitude in the free massive theory, given simply by

$$\mathcal{A}_0 = \langle \phi = 0 | e^{-H_0\tau_0} | \phi = 0 \rangle = \mathcal{N} [\det(-\square + m^2)]^{-1/2}. \quad (\text{C.9})$$

¹⁸Let us neglect the cosmological constant renormalization as it does not affect the energy splitting.

In the ratio of the two amplitudes the normalization factor cancels:

$$\mathcal{A}_-/\mathcal{A}_0 \approx \kappa\tau_0, \quad \kappa = \sqrt{\frac{S_0}{2\pi}} e^{-S_0} \left[\frac{\det'(-\square + V'')}{m^{-2} \det(-\square + m^2)} \right]^{-1/2} m. \quad (\text{C.10})$$

Now, let us calculate the determinant ratio. We need to solve the eigenvalue equation:

$$\left(-\frac{d^2}{dx^2} - \frac{d^2}{d\tau^2} + 12g\phi_0^2 - 4gc^2 \right) \psi = \left(-\frac{d^2}{dx^2} - \frac{d^2}{d\tau^2} + m^2 - \frac{3}{2}m^2 \frac{1}{\cosh^2 \frac{m\tau}{2}} \right) \psi = \epsilon\psi. \quad (\text{C.11})$$

The eigenstates are of the form $\psi(x, \tau) = e^{-ik_n x} \psi_n(\tau)$, where $k_n = \frac{2\pi n}{L}$ due to periodic boundary condition on the cylinder, and

$$\left(-\frac{d^2}{d\tau^2} + \omega_n^2 - \frac{3}{2}m^2 \frac{1}{\cosh^2 \frac{m\tau}{2}} \right) \psi_n = \epsilon_n \psi_n, \quad (\text{C.12})$$

where we defined $\omega_n^2 \equiv k_n^2 + m^2$. The eigenvalues of (C.12) comprise two bound states:

$$\epsilon_{n,0} = k_n^2, \quad \epsilon_{n,1} = \frac{3}{4}m^2 + k_n^2 \quad (\text{C.13})$$

and a continuum (for infinite τ_0) of states with $\epsilon_n \geq \omega_n^2$ [41], which can be parametrized by the ‘‘momentum’’:

$$p = \sqrt{\epsilon_n} - \omega_n \geq 0. \quad (\text{C.14})$$

We consider $\tau_0 \gg m^{-1}$ large but finite (but not too large—see below). Imposing the boundary conditions $\psi_n(\pm\tau_0/2) = 0$, the p 's take discrete values:

$$p\tau_0 - \delta_p = \pi l = \tilde{p}_l \tau_0, \quad l = 0, 1, \dots \quad (\text{C.15})$$

where the \tilde{p}_l represent the eigenvalues in the free theory, and the phase shift is [41]:

$$\delta_p = -2\pi + 2 \arctan \frac{2p}{m} + 2 \arctan \frac{p}{m} \quad (\text{C.16})$$

Here the -2π term is added so that δ_p vanishes for $p \rightarrow \infty$, corresponding to the fact that the effects of the potential disappear at high energies. In fact only $l \geq 2$ gives $p \geq 0$, while for \tilde{p} we have $l \geq 0$. Taking into account the two bound states, we have the same number of eigenstates with and without the kink. The determinant ratio in (C.7) at large τ_0 evaluates to:

$$\frac{\det'(-\square + V'')}{m^{-2} \det(-\square + m^2)} = \prod_{n=-\infty}^{\infty} \left\{ \left(\frac{k_n^2}{\omega_n^2} \right)^{1-\delta_{n0}} \frac{k_n^2 + \frac{3}{4}m^2}{\omega_n^2} \prod_{l=2}^{\infty} \frac{p_l^2 + \omega_n^2}{\tilde{p}_l^2 + \omega_n^2} \right\}. \quad (\text{C.17})$$

We took into account that for $n = 0$ the first bound state of the kink theory is the zero mode which has been already factored out.

Performing the product over n by means of the identity:

$$\frac{\sinh z}{z} = \prod_{n=1}^{\infty} \left(1 + \frac{z^2}{\pi^2 n^2} \right), \quad (\text{C.18})$$

we can write the result in the form

$$\frac{\det'(-\square + V'')}{m^{-2} \det(-\square + m^2)} = (mL)^2 e^{mL(\frac{\sqrt{3}}{2}-2)+L\Sigma+2b}, \quad (\text{C.19})$$

$$\Sigma = \sum_{l=2}^{\infty} (p_l^2 + m^2)^{1/2} - (\tilde{p}_l^2 + m^2)^{1/2}, \quad (\text{C.20})$$

$$b = \log \frac{1 - e^{-\frac{\sqrt{3}}{2}mL}}{(1 - e^{-mL})^2} + \sum_{l=2}^{\infty} \log(1 - e^{-(p_l^2+m^2)^{1/2}L}) - \log(1 - e^{-(\tilde{p}_l^2+m^2)^{1/2}L}). \quad (\text{C.21})$$

For $\tau_0 m \gg 1$ we can approximate the sums by integrals:

$$\Sigma = \int_0^{\infty} \frac{dp}{\pi} \delta_p \frac{d}{dp} (p^2 + m^2)^{1/2} = m(2 - 3/\pi - 1/\sqrt{3}) + \log.\text{div.}, \quad (\text{C.22})$$

where the logarithmic UV divergence is canceled in the final answer by the counterterm in (C.5).

Analogously

$$b = \log \frac{1 - e^{-\frac{\sqrt{3}}{2}mL}}{(1 - e^{-mL})^2} + \int_0^{\infty} \frac{dp}{\pi} \delta_p \frac{d}{dp} \log(1 - e^{-(p^2+m^2)^{1/2}L}) = f(mL), \quad (\text{C.23})$$

$$f(x) = \log(1 - e^{-\frac{\sqrt{3}}{2}x}) - \frac{2}{\pi} \int_0^{\infty} dq \left(\frac{1}{1+q^2} + \frac{2}{1+4q^2} \right) \log(1 - e^{-(q^2+1)^{1/2}x}). \quad (\text{C.24})$$

The function $f(x)$ tends to zero exponentially fast for $x \gg 1$, whereas for intermediate x it has to be computed numerically, see figure 11.

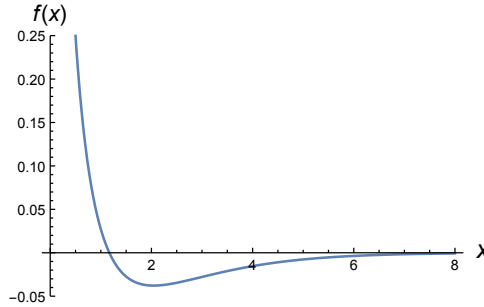


Figure 11: The function $f(x)$ defined in Eq. (C.24).

Gathering everything, the coefficient κ in (C.10) is given by (cf. [40], (3.27))

$$\kappa = \sqrt{\frac{m^3}{24\pi gL}} e^{-LM_{\text{kink}} - f(mL)}, \quad M_{\text{kink}} = \frac{m^3}{12g} + m \left(\frac{1}{4\sqrt{3}} - \frac{3}{2\pi} \right). \quad (\text{C.25})$$

Not surprisingly, the leading exponential dependence of this result is governed by the kink mass M_{kink} in the one-loop approximation, first computed in [26].

The one-instanton approximation for \mathcal{A}_- will break down for τ_0 so large that $\kappa\tau_0 = O(1)$. In this extreme $\tau_0 \rightarrow \infty$ limit, both amplitudes \mathcal{A}_\pm receive contributions from multi-instanton configurations in the path integral, which are approximate solutions of the equation of motion. We can use the instanton-gas approximations, where the centers of the instantons are far apart, and resum all these contributions, to give:

$$\mathcal{A}_+ = \mathcal{A}_0 \cosh \kappa\tau_0, \quad \mathcal{A}_- = \mathcal{A}_0 \sinh \kappa\tau_0. \quad (\text{C.26})$$

We did not consider the purely perturbative corrections to these amplitudes, as they are the same for the quasi-degenerate states and therefore do not interest us.

Taking the $\tau_0 \rightarrow \infty$ limit in (C.26), one can infer the presence of two exchanged states split in energy by $\Delta\mathcal{E} = 2\kappa$, which is our final result.

References

- [1] S. Rychkov and L. G. Vitale, “Hamiltonian truncation study of the ϕ^4 theory in two dimensions,” *Phys. Rev.* **D91** no. 8, (2015) 085011, [arXiv:1412.3460 \[hep-th\]](#).
- [2] S.-J. Chang, “The Existence of a Second Order Phase Transition in the Two-Dimensional ϕ^4 Field Theory,” *Phys.Rev.* **D13** (1976) 2778.
- [3] A. Coser, M. Beria, G. P. Brandino, R. M. Konik, and G. Mussardo, “Truncated Conformal Space Approach for 2D Landau-Ginzburg Theories,” *J. Stat. Mech.* **1412** (2014) P12010, [arXiv:1409.1494 \[hep-th\]](#).
- [4] V. P. Yurov and Al. B. Zamolodchikov, “Truncated Conformal Space Approach to Scaling Lee-Yang Model,” *Int.J.Mod.Phys.* **A5** (1990) 3221–3246.
- [5] M. Lassig, G. Mussardo, and J. L. Cardy, “The scaling region of the tricritical Ising model in two-dimensions,” *Nucl.Phys.* **B348** (1991) 591–618.
- [6] B. Simon, *The p (ϕ) in Two-Dimensions Euclidean (Quantum) Field Theory*. 1974.
- [7] W. Loinaz and R. Willey, “Monte Carlo simulation calculation of critical coupling constant for continuum ϕ^4 in two-dimensions,” *Phys.Rev.* **D58** (1998) 076003, [arXiv:hep-lat/9712008 \[hep-lat\]](#).
- [8] D. Schaich and W. Loinaz, “An improved lattice measurement of the critical coupling in ϕ_2^4 theory,” *Phys.Rev.* **D79** (2009) 056008, [arXiv:0902.0045 \[hep-lat\]](#).
- [9] C. Wozar and A. Wipf, “Supersymmetry Breaking in Low Dimensional Models,” *Annals Phys.* **327** (2012) 774–807, [arXiv:1107.3324 \[hep-lat\]](#).
- [10] P. Bosetti, B. De Palma, and M. Guagnelli, “Monte Carlo determination of the critical coupling in ϕ_2^4 theory,” *Phys. Rev.* **D92** no. 3, (2015) 034509, [arXiv:1506.08587 \[hep-lat\]](#).
- [11] A. Harindranath and J. Vary, “Solving Two-Dimensional ϕ^4 Theory By Discretized Light Front Quantization,” *Phys.Rev.* **D36** (1987) 1141–1147.
- [12] T. Sugihara, “Density matrix renormalization group in a two-dimensional lambda ϕ^4 Hamiltonian lattice model,” *JHEP* **0405** (2004) 007, [arXiv:hep-lat/0403008 \[hep-lat\]](#).
- [13] A. Milsted, J. Haegeman, and T. J. Osborne, “Matrix product states and variational methods applied to critical quantum field theory,” *Phys.Rev.* **D88** (2013) 085030, [arXiv:1302.5582 \[hep-lat\]](#).

- [14] D. Lee, N. Salwen, and D. Lee, “The Diagonalization of quantum field Hamiltonians,” *Phys.Lett.* **B503** (2001) 223–235, [arXiv:hep-th/0002251 \[hep-th\]](#).
- [15] D. Lee, N. Salwen, and M. Windolowski, “Introduction to stochastic error correction methods,” *Phys.Lett.* **B502** (2001) 329–337, [arXiv:hep-lat/0010039 \[hep-lat\]](#).
- [16] A. Pelissetto and E. Vicari, “Critical mass renormalization in renormalized ϕ^4 theories in two and three dimensions,” *Phys. Lett.* **B751** (2015) 532–534, [arXiv:1508.00989 \[hep-th\]](#).
- [17] S. R. Coleman, “The Quantum Sine-Gordon Equation as the Massive Thirring Model,” *Phys.Rev.* **D11** (1975) 2088.
- [18] P. Giokas and G. Watts, “The renormalisation group for the truncated conformal space approach on the cylinder,” [arXiv:1106.2448 \[hep-th\]](#).
- [19] G. Feverati, K. Graham, P. A. Pearce, G. Z. Toth, and G. Watts, “A Renormalisation group for TCSA,” *J. Stat. Mech.* (2008) P03011, [arXiv:hep-th/0612203 \[hep-th\]](#).
- [20] G. M. Watts, “On the renormalisation group for the boundary Truncated Conformal Space Approach,” *Nucl.Phys.* **B859** (2012) 177–206, [arXiv:1104.0225 \[hep-th\]](#).
- [21] M. Lencses and G. Takacs, “Excited state TBA and renormalized TCSA in the scaling Potts model,” *JHEP* **09** (2014) 052, [arXiv:1405.3157 \[hep-th\]](#).
- [22] M. Hogervorst, S. Rychkov, and B. C. van Rees, “Truncated conformal space approach in d dimensions: A cheap alternative to lattice field theory?,” *Phys. Rev.* **D91** (2015) 025005, [arXiv:1409.1581 \[hep-th\]](#).
- [23] M. Caselle, M. Hasenbusch, P. Provero, and K. Zarembo, “Bound states in the three-dimensional ϕ^4 model,” *Phys.Rev.* **D62** (2000) 017901, [arXiv:hep-th/0001181 \[hep-th\]](#).
- [24] M. Lüscher, “Volume Dependence of the Energy Spectrum in Massive Quantum Field Theories. 1. Stable Particle States,” *Commun.Math.Phys.* **104** (1986) 177.
- [25] G. Delfino, G. Mussardo, and P. Simonetti, “Nonintegrable quantum field theories as perturbations of certain integrable models,” *Nucl. Phys.* **B473** (1996) 469–508, [arXiv:hep-th/9603011 \[hep-th\]](#).
- [26] R. F. Dashen, B. Hasslacher, and A. Neveu, “Nonperturbative Methods and Extended Hadron Models in Field Theory. 2. Two-Dimensional Models and Extended Hadrons,” *Phys. Rev.* **D10** (1974) 4130–4138.
- [27] G. Mussardo, “Neutral Bound States in Kink-like Theories,” *Nucl. Phys.* **B779** (2007) 101–154, [arXiv:hep-th/0607025 \[hep-th\]](#).
- [28] Z. Bajnok and M. Lajer, “Truncated Hilbert space approach to the 2d ϕ^4 theory,” [arXiv:1512.06901 \[hep-th\]](#).
- [29] J. Elias-Miro, M. Montull, and M. Riembau, “The renormalized Hamiltonian truncation method in the large E_T expansion,” [arXiv:1512.05746 \[hep-th\]](#).
- [30] Z. Bajnok, L. Palla, G. Takács, and F. Wagner, “Nonperturbative study of the two frequency sine-Gordon model,” *Nucl.Phys.* **B601** (2001) 503–538, [arXiv:hep-th/0008066 \[hep-th\]](#).
- [31] P. Fonseca and A. Zamolodchikov, “Ising spectroscopy. I. Mesons at $T < T_c$,” [arXiv:hep-th/0612304 \[hep-th\]](#).
- [32] J.-S. Caux and R. M. Konik, “Constructing the generalized Gibbs ensemble after a quantum quench,” *Phys. Rev. Lett.* **109** (2012) 175301, [arXiv:1203.0901 \[cond-mat.quant-gas\]](#).

- [33] G. P. Brandino, J.-S. Caux, and R. M. Konik, “Glimmers of a Quantum KAM Theorem: Insights from Quantum Quenches in One Dimensional Bose Gases,” [arXiv:1407.7167](#) [[cond-mat.str-el](#)].
- [34] R. M. Konik, T. Pálmai, G. Takács, and A. M. Tsvelik, “Studying the perturbed Wess-Zumino-Novikov-Witten $SU(2)_k$ theory using the truncated conformal spectrum approach,” *Nucl. Phys.* **B899** (2015) 547–569, [arXiv:1505.03860](#) [[cond-mat.str-el](#)].
- [35] L. Lepori, G. Z. Toth, and G. Delfino, “Particle spectrum of the 3-state Potts field theory: A Numerical study,” *J. Stat. Mech.* **0911** (2009) P11007, [arXiv:0909.2192](#) [[hep-th](#)].
- [36] M. Lencsés and G. Takács, “Confinement in the q -state Potts model: an RG-TCSA study,” *JHEP* **09** (2015) 146, [arXiv:1506.06477](#) [[hep-th](#)].
- [37] I. Brooks, E.D. and S. C. Frautschi, “Scalars Coupled to Fermions in (1+1)-dimensions,” *Z.Phys.* **C23** (1984) 263.
- [38] M. Serone, G. Spada, and G. Villadoro, “ $\lambda\phi^4_2$ Theory II: The Broken Phase Beyond NNNN(NNNN)LO,” [arXiv:1901.05023](#) [[hep-th](#)].
- [39] A. I. Vainshtein, V. I. Zakharov, V. A. Novikov, and M. A. Shifman, “ABC of Instantons,” *Sov. Phys. Usp.* **25** (1982) 195. [*Usp. Fiz. Nauk* 136, 553 (1982)].
- [40] H. Osborn, “Partition Function For Two-Dimensional Solitons,” *Nucl. Phys.* **B143** (1978) 327.
- [41] P. M. Morse and H. Feshbach, *Methods of Theoretical Physics*. McGraw-Hill, New York, 1953. part II, ch.12, p.1651.